Optimization of an Adamantane Thruster for CubeSat Deorbiting

IEPC-2025-442

Presented at the 39th International Electric Propulsion Conference
Imperial College London • London, United Kingdom
14-19 September 2025

Olivia Kukar[*], Jonathan Fisher[†], Cameron Coen[‡], Autumn Zaretsky[§], Nicholas Kiley[**], Max Wu[††], Matthew Gilpin[‡‡], and Lubos Brieda[§§]
University of Southern California, Los Angeles, CA, 90007, USA

Abstract: The recent increase in CubeSat launches and the FCC's 5-year deorbit requirement has created a demand for compact, low-power electric propulsion systems capable of propulsive deorbiting. Adamantane ($C_{10}H_{16}$) is a promising propellant for nano-satellite active deorbiting systems because of its solid nature at room temperature, low ionization voltage, and high vapor pressure, removing the need for pressurized storage and heating systems. This study reports results from an experimental investigation of adamantane's performance in an ion thruster design. Four different thruster geometries were tested on a torsional thrust stand, yielding values of 20 ± 6 μN at 1.9 ± 0.3 W, within typical CubeSat power budgets. Testing also revealed critical contamination issues with adamantane, resulting in significant carbon deposition that degraded thruster performance and prevented reliable plasma diagnostics. Comprehensive material testing demonstrated that glass construction mitigates this buildup and restores diagnostic capability. Langmuir probe diagnostics using adamantane plasma yielded electron densities of $1.4 \cdot 10^{17}$ m^{-3} $\pm$ $4 \cdot 10^{16}$ m^{-3} and temperatures of 3.0 ± 0.4 eV, confirming adamantane's potential use as a fuel for electric propulsion. The following work explores the feasibility of adamantane as an alternative propellant in electric propulsion, establishing clear design principles for the next phase of ASPEN's thruster development.

[*] Graduate Student, Viterbi School of Engineering, okukar@usc.edu.
[†] Undergraduate Student, Viterbi School of Engineering, fisherjr@usc.edu.
[‡] Undergraduate Student, Viterbi School of Engineering, ccoen@usc.edu.
[§] Undergraduate Student, Viterbi School of Engineering, azartsk@usc.edu.
[**] Undergraduate Student, Viterbi School of Engineering, nkiley@usc.edu.
[††] Undergraduate Student, Dornsife School of Arts and Sciences, mxwu@usc.edu.
[‡‡] Associate Professor of Aerospace and Mechanical Engineering Practice, Viterbi School of Engineering, gilpin@usc.edu.
[§§] Part-time Lecturer of Astronautical Engineering (USC), now at Cal Poly San Luis Obispo lbrieda@calpoly.edu.

Nomenclature

F_t = thrust
I_{sp} = specific impulse
$\dot{m}$ = mass flow
v_e = exit velocity
I_i = ion beam current
m_i = ion mass
q_i = ion charge
V_0 = potential difference
I_d = applied current
η_b = current utilization efficiency
n_e = electron density
T_e = electron temperature
Φ_p = plasma potential
Φ_f = floating potential

I. Introduction

There is a need for small, compact, low-power electric propulsion devices for deorbiting CubeSats. With a 5-year deorbit required imposed on satellites by the FCC, nanosatellites in higher-altitude LEO orbits can no longer rely on drag to deorbit them within the allowable timeframe.[1] Though certain passive deorbit systems show promise for application on nano- and picosatellites, active deorbit systems allow for greater control over deorbit maneuvers[2]. Current projections estimate that a 3U CubeSat with a mass of 4 kg can take over 25 years to naturally decay from orbit when operating at altitudes of 600 km.[3] To deorbit a satellite under these parameters, an active deorbit system must apply approximately 225 m/s of ΔV, bringing the satellite to an orbital radius of 180km. At that altitude, drag effects dominate to complete the deorbit process within a matter of hours.[4] While operating with 200 grams of propellant, a minimum I_{sp} of roughly 1170 seconds is required for this maneuver.

These deorbit I_{sp} requirements pose significant storage challenges for common alternative propulsion systems. Gaseous propellants demand significant concessions of mass and volume for high-pressure storage systems in nanosatellite design. Alternatively, solid propellant allows for more compact feed systems with higher ΔV-to-volume ratios. Solid propellants do not require propellant feeds or tanks, significantly reducing complications when designing sufficiently small thrusters. This ease of miniaturization is vital when developing active deorbit systems for nanosatellite form factors.

Adamantane ($C_{10}H_{16}$) has been proposed and studied as an alternative propellant. This propellant is solid at standard temperature and easily ionized, with an ionization energy of 9.75 eV.[5] Under temperatures of 293 K, adamantane sublimates at a pressure of 93 mTorr[6]. This vapor pressure eliminates the need for high-pressure storage, heaters, or a catalyst bed in an adamantane-based thruster, offering the potential for a simple, high-density, low-mass design. For comparison, Xenon must be stored at a pressure of over 7 mPa[7] to have a comparable density to solid adamantane, requiring significant equipment with further volume requirements.

Previous studies have examined adamantane's feasibility with varying results. They find that it may serve as a viable molecular propellant for thrusters due to its ability to ionize, but it still faces challenges such as carbon deposition and unstable plasma.[8, 9, 10] More research is needed to investigate how adamantane acts when used as fuel for a thruster.

The Advanced Spacecraft Propulsion and Energy (ASPEN) Lab at the University of Southern California is developing a simple adamantane-fueled plasma thruster to explore adamantane's viability as a propellant for EP applications and develop ASPEN's thrust measurement and plasma diagnostic capabilities. A simple, large-scale thruster was manufactured and tested to guide future design principles to be integrated onto a 3U CubeSat platform.

To characterize the performance of this thruster, a torsional thrust stand and a Langmuir probe were constructed. ASPEN then used these diagnostics to evaluate different geometries to optimize thruster performance. The results of this testing will inform future thruster designs, which are to be implemented on a nanosatellite platform.

II. Thruster Design

The ASPEN plasma thruster is designed to ionize and expel adamantane propellant while utilizing only a few components for simplicity. Presently, the thruster is designed at a larger scale than would be suitable for CubeSat integration. ASPEN is still developing its lab capabilities, and a larger thruster design enables easier manufacturing with the in-house tools available. Additionally, the current goal of ASPEN is to rapidly iterate between designs and understand how adamantane acts as an EP propellant. To be successfully implemented in space, the final design will be smaller, with geometry and material selection informed by the results of this study and future investigation.

A. Operating Principles

The thruster is composed of a propellant tank, ionization chamber, anode, cathode, and orifice, as shown in Figure 1. Solid adamantane powder is stored in the propellant tank prior to firing. The propellant is directly exposed to the ionization chamber.

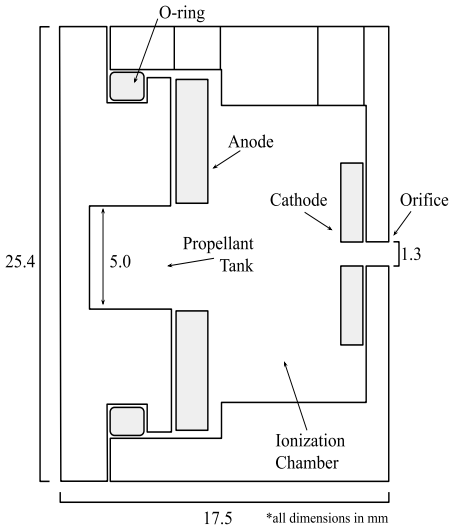

Figure 1. ASPEN thruster diagram. Adamantane is stored as a solid powder in the propellant tank and sublimates into a vapor, where it is ionized and accelerated in the ionization chamber.

Adamantane's sublimation pressure at room temperature, 93 mTorr,[6] allows the adamantane powder to sublimate readily during testing and enter the ionization chamber. Plasma is ignited when the local conditions within the ionization chamber meet breakdown voltage criteria for the adamantane vapor.

The electrodes are spaced 6.35 mm apart, creating an electric field strength of 126 kV/m. In the ideal case, electrons could be accelerated to obtain a maximum possible energy of 800 eV, which is sufficient to ionize adamantane molecules through collision, as adamantane's ionization energy is 9.75 eV.[5] Ionization is sustained throughout the duration of the thruster firing.

The thruster was manufactured with 3D printing, constructed from a clear photopolymer resin mixture, primarily urethane dimethacrylate. This material was selected due to its inexpensive nature and quick manufacturing times. Despite concerns about this clear resin's high outgassing rate, these traits were prioritized to allow for rapid adjustments to the thruster geometry, expediting optimization. Following geometrical optimization of the thruster, future iterations using the final thruster design will be manufactured with lower outgassing materials.

B. Variable Geometry

While the operating principles remained the same for all tests, a comparative study was conducted to evaluate how the internal thruster geometry and electrode design affected the thruster's efficiency. All testing for this study was conducted using thrusters made from the 3D-printed resin, again chosen for ease of iterability and cost effectiveness. Four configurations were tested. Each model is displayed in Figure 2 below.

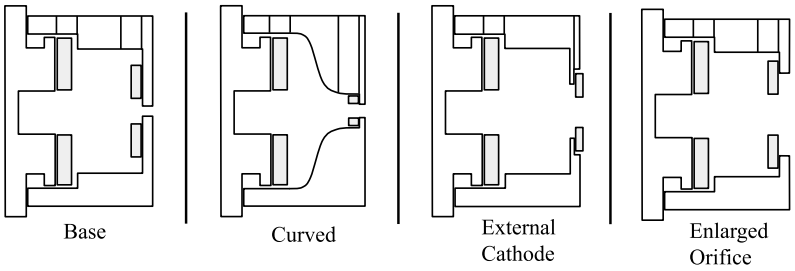

Figure 2. Variable geometries characterized during experimental testing.

The base model, with a simple rectangular interior, served as a control model, having demonstrated reliable ignition in earlier tests. A curved variation was designed with a smaller cathode to attempt to direct the ions through the orifice with a more focused electric field. The enlarged orifice configuration tested whether increasing the orifice size would allow for higher flow rates and increased thrust, though there were concerns about potential instability. The final configuration, external cathode, was inspired by the need to reduce cathode carbon buildup observed in earlier designs. By placing the cathode outside of the ionization chamber, it was expected that the cathode would be exposed to fewer high-velocity ions, reducing contamination.

III. Diagnostic Capabilities

To characterize the performance of the different thruster geometries and understand the behavior of adamantane as a propellant, diagnostic equipment was developed. ASPEN's current diagnostic suite consists of a thrust stand and a Langmuir probe.

A. Thrust Stand Overview

The ASPEN torsional thrust stand was developed to improve upon the laboratory's earlier hanging pendulum measurements by providing greater sensitivity and stability in a configuration compatible with the lab's vacuum chamber. The stand, shown in Figure 3 below, was constructed following a torsional design as described in Polk et al[10].

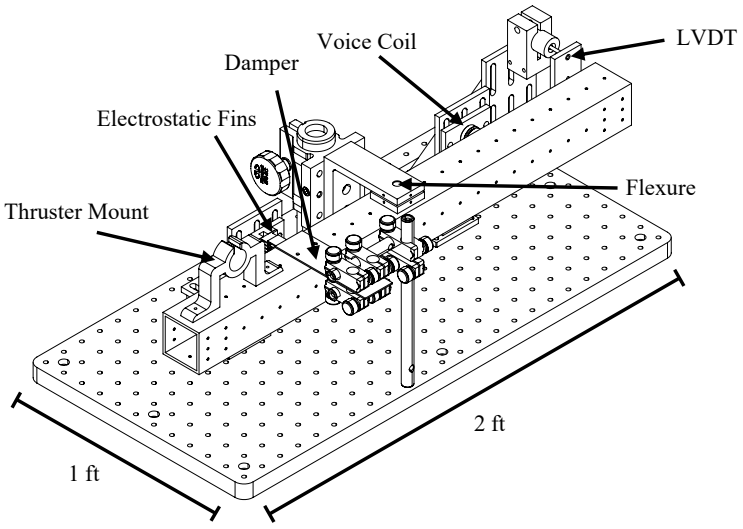

Figure 3. A schematic of the ASPEN torsional thrust stand. Note that aluminum shielding and thruster cables are not shown.

The stand consists of a 2-foot aluminum balance beam supported at its midpoint by two precision flex pivots, each having a spring constant of 0.311 N·m/rad. The thruster is mounted at one end of the arm and imparts a torque on the beam when fired. A voice coil actuator mounted on the opposite side of the pivot point holds the beam in a steady, zero position, as shown in Figure 4 below. Displacement, measured by a linear variable differential transformer (LVDT), serves as feedback for the voice coil, which uses a proportional–integral–derivative (PID) control loop to maintain the null position. Damping is provided by both the PID controller and a passive magnetic current damper to reduce controller derivative noise.

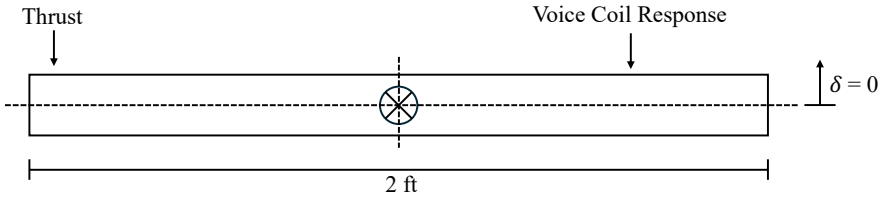

Figure 4. Null balance thrust stand configuration. Torque applied to one side of the pivot point is counteracted by the voice coil actuator, resulting in zero steady-state displacement of the beam.

Thrust is determined from the electric current applied to the voice coil to maintain the null position. This current is supplied via a unity gain op amp circuit and measured across a resistor placed in series with the coil. To calibrate the system and develop a conversion factor between applied torque on the beam and current in the voice coil, electrostatic fins were employed. Following the practices outlined by Polk et al, steady-state high voltage pulses are applied to a set of overlapping aluminum fins[10]. These voltages create electrostatic forces, which were previously empirically characterized.[12] These forces impart known torques on the beam, which are counteracted by the PID control loop and the voice coil, as shown in Figure 5 below.

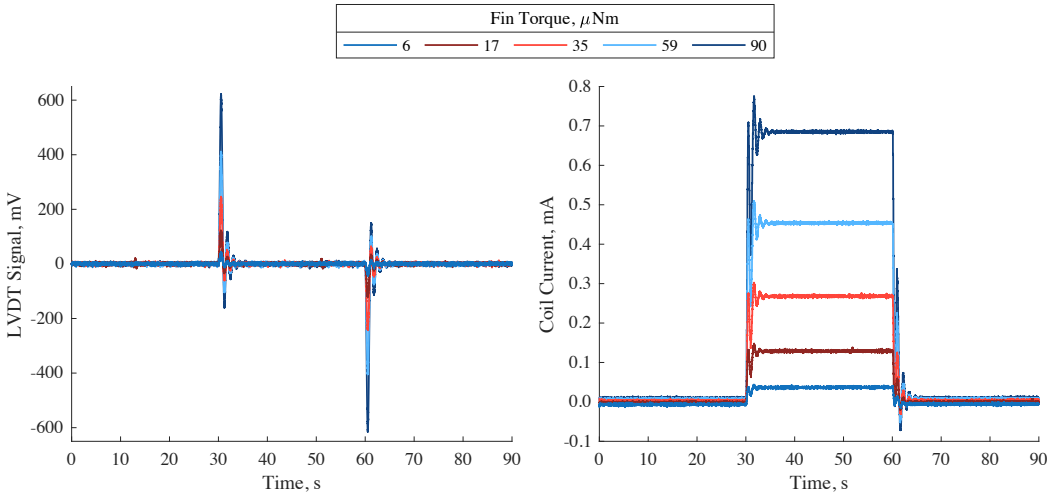

Figure 5. Example calibration procedure. The LVDT signal is held at zero by the voice coil actuator when a torque is applied by the electrostatic calibration fins.

The steady-state voice coil current profiles allow for a calibration curve to be generated relating the current to the known torque on the beam. An example calibration curve is shown in Figure 6.

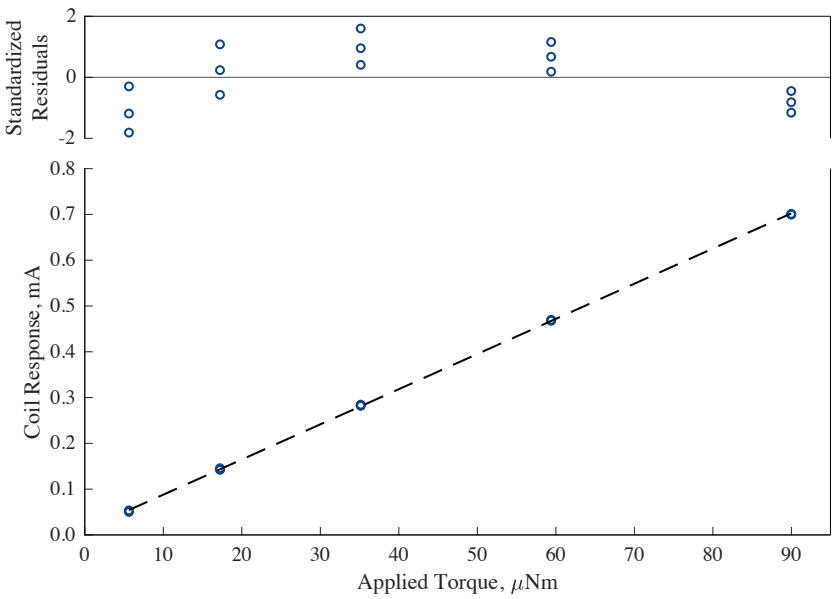

Figure 6. Example calibration curve. Voice coil current is directly proportional to torque applied to the beam.

There is a linear relationship between the applied torque and coil response, allowing for direct proportional conversion between the coil response and thrust.

During testing, calibrations were performed at atmospheric conditions to prevent premature sublimation of propellant. Calibrations at atmosphere and in vacuum were compared and shown to differ by less than 2% so there is confidence that the thrust stand calibration is stable after pump down and during testing.

B. Langmuir Probe Overview

In addition to characterizing the thrust of the adamantane-fueled system, a Langmuir probe was developed in-house by the ASPEN Lab to characterize the plasma of ASPEN's thruster.

Inspired by Polk et al.[12], the probe's collecting surface was a tantalum sheet spot-welded to a nickel-chromium wire insulated by alumina.[13] Utilizing a waveform generator, a sawtooth signal from -28.4 V to 28.4 V was applied to the Langmuir probe with a frequency of 10 Hz. Data was collected by measuring voltage differentials over a resistor using a NI USC-6211 DAQ and processed in MATLAB. 100 voltage sweeps at 10 Hz were averaged together to provide a resulting I-V curve and minimize the impact of outliers.

To ensure accuracy, the procedures outlined in Polk et al.[12] to collect and analyze probe data were followed. Recommended practices for utilizing Langmuir probes in electric propulsion applications were followed to the extent possible.[14] Due to the limitations of ASPEN's single-probe construction, ASPEN was unable to utilize a high-speed dual Langmuir probe. Regardless, adherence to the recommended practices in Polk et al.[12] and following material and analytical recommendations in Gilpin et al.[13] gives confidence in order-of-magnitude estimates derived from Langmuir probe measurements.

IV. Thruster Testing

The thruster was tested in ASPEN's vacuum chamber using both the thrust stand and the Langmuir probe. It was fired at a back pressure of $1 \cdot 10^{-4}$ Torr. Additionally, during firing, the power supply was limited to 2 mA of current. Under these conditions, the thrust stand provided insight into the thruster's performance, and the Langmuir probe contributed to the lab's understanding of adamantane's behavior as a propellant and the material requirements for the thruster.

C. Thrust Stand Measurements

The four geometries were tested on the thrust stand with varying degrees of success. The base thruster proved to be the most reliable geometry, igniting and maintaining stable operating conditions. The curved geometry showed inconsistent behavior, and arcing in the thruster resulted in instabilities in the data collection system; it was unable to maintain a stable, current-limited condition during firing. With the other two geometries, the external cathode and large orifice, ignition was unsuccessful. Due to both geometries having larger orifices, the necessary chamber pressure for ignition could not be reached, and plasma was not ignited. No arcing was observed for those two geometries.

While three of the geometries were unsuccessful, the base geometry's thrust was measured by the thrust stand. A representative thrust profile from a base thruster test is displayed in Figure 7 below.

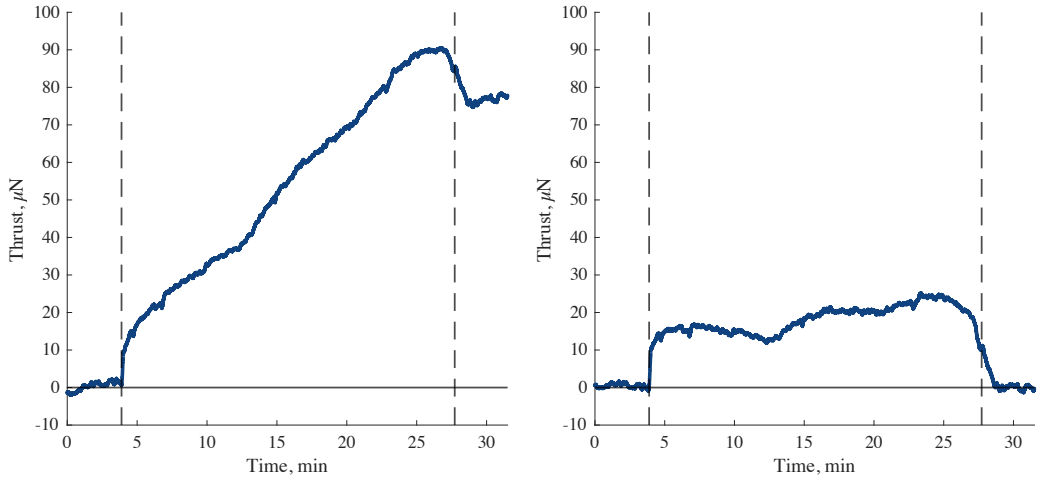

Figure 7. Representative thrust data for the base geometry. The graph on the left displays raw data, and the graph on the right displays the thrust profile after removing linear drift. An average of 18 μN of thrust was measured during this test. Note that the dashed lines indicate where power to the thruster was switched on and off, and a 6-second moving average filter was applied to the data.

During the development of the thrust stand, steps were taken to eliminate sources of error and drift. To eliminate electrostatic effects from the two cables providing power to the thruster, thin coaxial cables were used. These cables were draped down to the beam and anchored near the pivot point to reduce any torque they could have on the system. Additionally, an aluminum wall was added between the thruster and the rest of the stand to create a large grounding plane, preventing charge buildup on any components. However, drift was still observed in the thrust data during testing. This drift was ultimately attributed to external torque applied to the beam by gravity.

The beam rotates around the flexures in its center. In the ideal case, the beam would be completely level, and the center of mass would be positioned at the flexures. The gravity force vector would be aligned with the rotation axis at the center of mass. Positioned directly at the flexures, it would impart no torque on the stand.

In the case of the ASPEN stand, there is no auto-leveling system. As a result, it is impossible to maintain the ideal level position, and when the stand is tilted, the rotation axis loses parallelism with the gravity vector. Furthermore, the stand is not balanced; the mass distribution across the beam is asymmetrical. This imbalance shifts the center of mass away from the rotation axis. Because of these two misalignments, the gravity force, acting at the center of mass, imparts a torque on the beam with a component perpendicular to the rotation axis, as displayed in Figure 8.

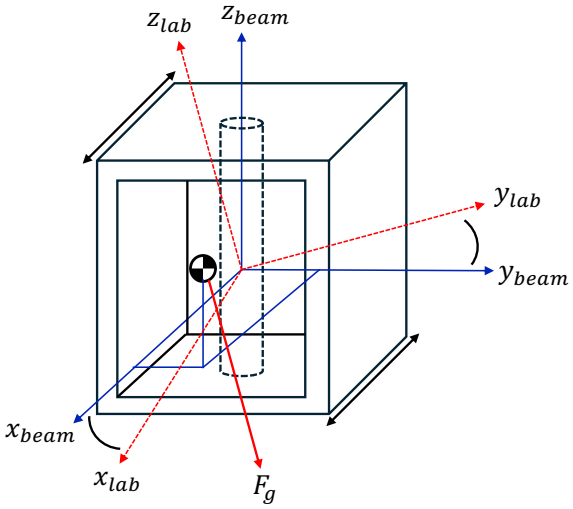

Figure 8. Center of mass misalignment, beam tilt, and gravitational torque shown at the rotation axis of the beam. Due to the beam's tilt and uneven mass distribution, gravity, acting at the center of mass, torques the beam. A component of this torque, in the direction of thrust, affects the thrust stand measurements. As the center of mass shifts due to propellant loss, the torque changes, causing drift.

The magnitude of this gravity induced torque changed as the mass distribution across the beam changed during testing, creating the linear drift that was observed in the data. When propellant sublimated and left the thruster, the mass at the thrust end of the beam decreased, and as a result, the center of mass shifted, altering the strength of the gravity induced torque on the beam.

During pump down, due to the propellant tank being exposed to the ambient pressure in the vacuum chamber, adamantane began sublimating prior to thruster ignition. This premature, passive propellant loss, while not creating a measurable thrust, did cause drift in the system because of the effects described above. When the thruster was ignited, the drift increased significantly, suggesting higher sublimation rates and mass flow from the thruster. Finally, after firing, as any residual adamantane remaining in the thruster sublimated, drift was observed again at a similar rate as before firing. In long duration tests, this final drift eventually leveled out as all propellant was exhausted and mass distribution remained the same across the beam. The linear drift approximations are displayed in Figure 9.

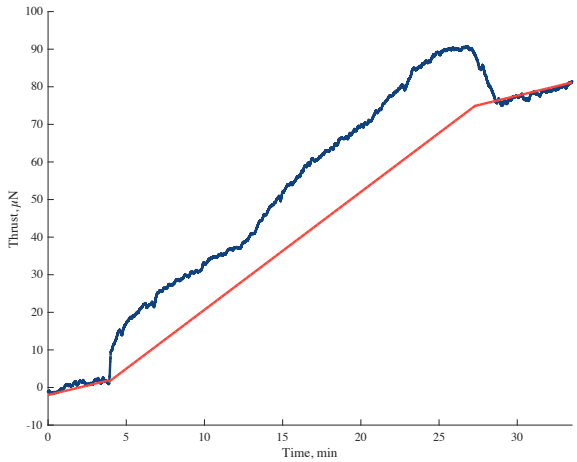

Figure 9. Linear drift visualization. Drift (red line), was caused by mass loss during testing as propellant sublimated. The sublimation rate increased during firing due to plasma interaction with the propellant.

In the test displayed in Figure 9, there was an observed drift of about 80 μN. The thruster was weighed before and after firing, with a total change in mass of 0.18 g. To confirm that the observed drift was caused by the center of mass shifting, a 0.2 g mass was placed on the thruster mount, and the resulting force measurement was within an order of magnitude of 80 μN. This test was performed in ambient conditions without the vacuum chamber door closed, exposing the stand to air currents that made a definitive force value difficult to obtain. As a result, more experimentation will have to be conducted to fully characterize this error source. Nevertheless, after subtracting the linear error described above, a clear thrust profile was created, as shown in Figure 7.

Additionally, power supply data was recorded, providing thruster input power measurements. Thrusters were tested until they expended all propellant and their power dropped to 0 W as ionization ceased within the chamber. The thrusters required relatively constant input power from the power supply during firing. A representative power trace is shown in Figure 11 below.

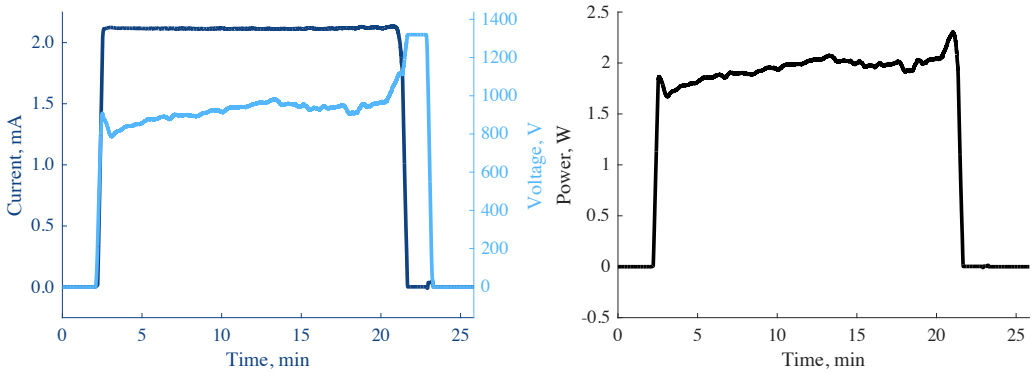

Figure 11. Representative power supply data for a thruster firing. The left graph displays voltage and current data, and the right graph displays power. Data is displayed with a 20 s moving average to reduce noise.

Like thrust data, power data has only been reliably obtained for the base thruster at this time. The base thruster was determined to have a thrust of 20 ± 6 μN and operate at a power of 1.9 ± 0.3 W.

D. Langmuir Probe Measurements

The base thruster geometry was also tested with the Langmuir probe, as shown in Figure 12; however, its design presented two key challenges during testing.

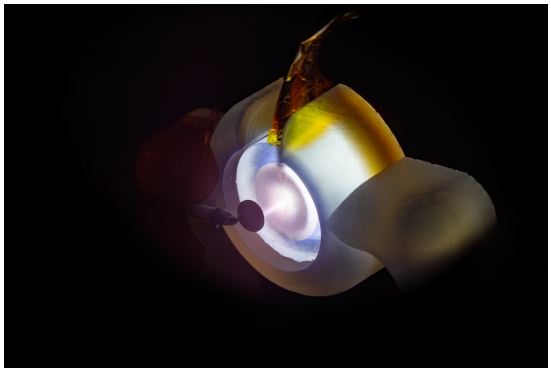

Figure 12. Langmuir probe testing on base resin thruster. Note the small diameter of the plume in relation to the probe tip.

The first challenge was making measurements in the small plume generated by the thruster. While its compact design is important for deployment onto CubeSats, the thruster generated a relatively small plume due to its small

geometry, as shown by the relative sizes of the plume and probe in Figure 12. As a result, the acquired results for plasma parameters likely vary from the true plasma values in an unperturbed plume because the relatively large surface area of the Langmuir probe perturbed the small plasma plume.[12] As such, the results acquired were viewed with caution. They provided an order-of-magnitude estimate to compare to simulation results and to ensure parameters of adamantane plasma were within the ranges of existing electric propulsion strategies.

The second problem was that the thruster contaminated the probe tip during operation. Initial Langmuir probe testing on the resin thruster presented such contamination qualitatively as a thin and uneven film forming on the tantalum probe tip (Figure 17). This film caused a dramatic increase in the resistance across the probe tip, measured with a multimeter. Before testing, the resistance across the probe tip was measured at 0.4 Ω. After testing, the DMM recorded a resistance of 5.7 kΩ. These contaminants degraded signal quality, increased probe failure rates, limited the duration and reliability of diagnostics, and ultimately prevented meaningful measurements from being collected on the resin thruster. To solve this contamination issue, thorough material testing and analysis was performed.

E. Contamination Study

Testing in ASPEN confirmed literature concerns about amorphous carbon deposits being a limiting factor for adamantane's implementation as a propellant; these deposits cause increased local arcing, reduce discharge uniformity, and alter the expected electrostatic field distribution.[15,16] Operation of the thruster in vacuum conditions led to significant carbon-related contamination, with implications for both performance degradation and hardware lifetime. After a few minutes of continuous discharge, carbon deposits were observed accumulating on the electrode surfaces. These black deposits formed in regions of intense plasma interaction, likely originating from adamantane decomposition and subsequent ionization. An example of this buildup is shown in Figure 13 below.

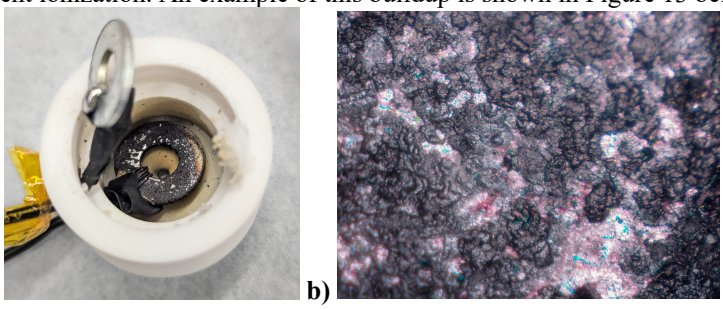

a) **b)**

Figure 13. a) Carbon buildup on a cathode observed post firing. b) Viewed through microscope.

Longer-duration tests of over 5 minutes resulted in the formation of a distinct white-to-gray crystalline residue within the thruster body and near the exhaust orifice, as shown in Figures 14 and 15. This crystal substance was submitted for Nuclear Magnetic Resonance (NMR) testing and single X-ray crystal diffraction. Some difficulty arose in performing these tests. The crystal structure did not dissolve well in benzene and instead needed to be treated with dimethyl sulfoxide (DMSO) and chloroform. This analysis revealed the residue to be a form of glass-like carbon, a non-graphitizing carbon material alongside trace amounts of water.

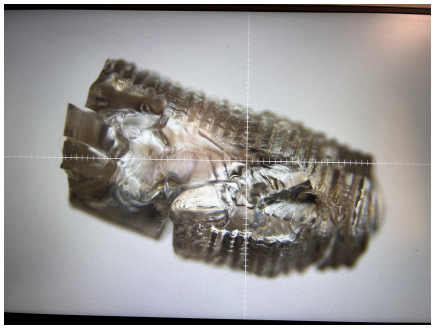

Figure 14. Glass-like carbon crystals found in initial testing at x20 magnification.

Glass-like carbon usually appears quite dark and opaque, unlike the image shown above. It's believed that this version of glass-like carbon appears more translucent due to surface texturing effects (powdering) and possible oxidation (surface oxidation from exposure to high temperatures in the thruster and other byproducts being formed).

Another point of note is the ridges formed along the edge of the crystal. These ridges (hexagon sheeting) do not match the texture on the side of the thruster nor any other surface in the ionization chamber. The hexagon sheeting effect seems to be from the compound deprotonating and forming a diamond-like structure. This formation would be extremely difficult without some medium to reorient and form these bonds, especially given the well-defined shapes and spacing. Most likely, trace amounts of silicon from vacuum grease or other contamination are present to act as this medium. The glass-like carbon material did not adhere strongly to surfaces, unlike the carbon deposits on the electrodes, but instead it accumulated loosely inside the thruster and was gradually expelled during operation.

A possible reason for the formation of this crystalline carbon form is adamantane's rigid, tetrahedral carbon structure, resembling the bonding in a diamond, which makes it well-suited to create diamond-like carbon (DLC) films. Studies have shown that when adamantane breaks down in plasma, it fragments into carbon clusters that retain diamond-like characteristics, which are more likely to recombine into ordered crystalline structures[17]. In the ASPEN thruster, interactions between plasma and un-sublimated adamantane could drive this fragmentation and reassembly process, explaining the presence of glass-like carbon.

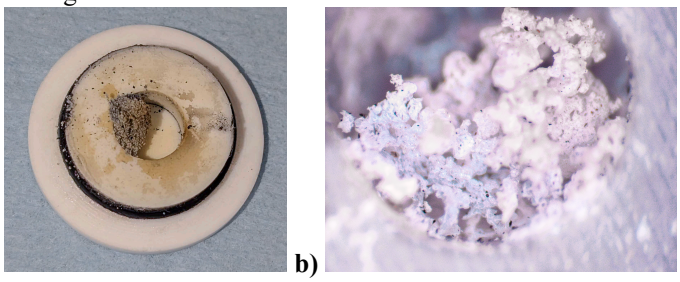

Figure 15. a) Glass-like carbon byproduct observed post firing. b) Viewed through a microscope.

It was also hypothesized that the thruster material influenced the formation of glass-like carbon, initiating a systematic material study. Lower-outgassing materials were experimented with to reduce both internal and external carbon contaminants. The original resin material's porosity and poor stability under vacuum led to excessive gas release. Therefore, a shift to Ultem resin, a high-performance polyetherimide known for its thermal stability and chemical resistance, was explored but ultimately proved unsuitable. Ultem increased crystalline accumulation, possibly because its 3D-printed structure contained internal voids that trapped residual adamantane, sustaining the formation of carbon-rich deposits. Only basic tests were performed using Ultem before the material was abandoned. The thruster was also tested using a glass-mica ceramic material (Macor), chosen for its machinability and affordability. However, this material also yielded glass-like carbon deposits during thruster tests.

An investigation was also performed to see if other materials present in the thruster could contribute to the formation of glass-like carbon. It was hypothesized that components such as zinc washers, plastic O-rings, and vacuum grease could be contributing trace outgassed solvents, which might serve as nucleation sites for carbon deposition. Zinc washers, which have a high off-gassing rate, were originally used for the cathode and anode due to their inexpensive nature and solderability. A shift was made to stainless steel washers, which have a much lower off-gassing rate, to see if this reduced the byproduct formation.[18] However, no noticeable change in deposits was observed.

Initial testing of the Langmuir probe system on a glass thruster iteration demonstrated the Langmuir probe system's ability to produce data[19]; the glass thruster also yielded no glass-like carbon. This result indicated that the excessive probe contamination preventing probe measurements on the original resin thruster correlated to the presence of glass-like carbon. While the glass thruster was the only iteration tested that yielded no glass-like carbon, amorphous carbon deposits were still present on the interior of the thruster, so the carbon deposit issue was not all-together mitigated using this material.

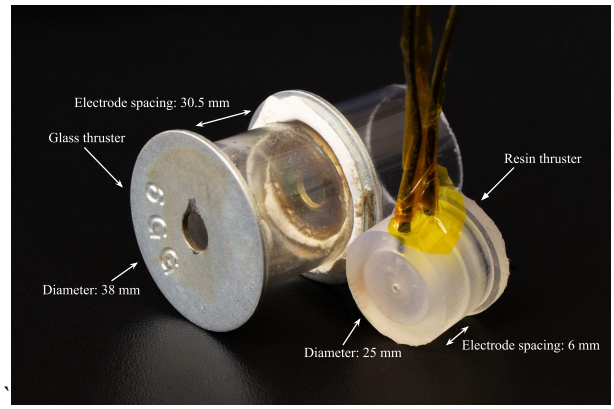

Figure 16. A comparison of the glass thruster (left) used for Langmuir probe data collection versus the resin thruster (right) used for thrust data collection

Ultimately, the glass thruster iteration, shown in Figure 16, was used with the Langmuir probe to acquire plasma data for adamantane. With this method, although the probe tip appeared anodized by the adamantane plasma, it maintained its conductivity with a measured resistance of 0.7 Ω after testing with the glass thruster. The glass thruster used to capture probe data was larger than other thrusters tested in this paper, both in diameter and chamber length. Electrode spacing in the ionization chamber was 30.5 mm with a potential of 1.4 kV, yielding a field strength of 46 kV/m. The plasma was generated by the same mechanism as with the original thruster design, but at a lower field strength. The plasma parameters obtained during glass thruster testing were used to estimate resin thruster performance; however, due to the lower field strength, these results likely underestimate the true performance of the resin thruster.

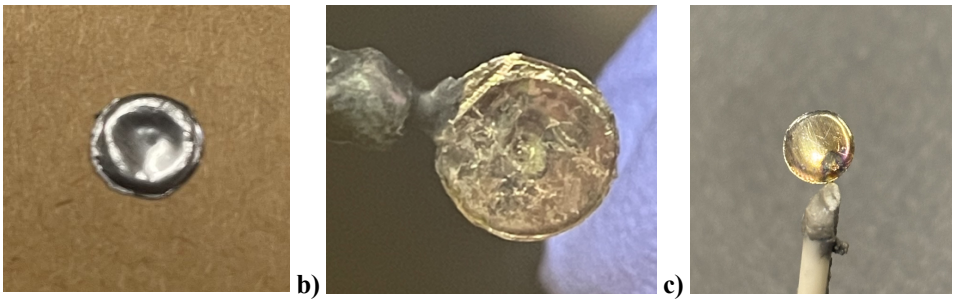

Figure 17. The tantalum probe tip used on the Langmuir probe a) before testing, b) after testing with a resin adamantane thruster, and c) after testing with a glass adamantane thruster.

Utilizing the Langmuir probe with a glass iteration of the thruster to reduce the glass-like carbon buildup on the probe and utilizing adamantane-fueled plasma proved successful. The resulting averaged I-V curves generated are shown in Figure 18.

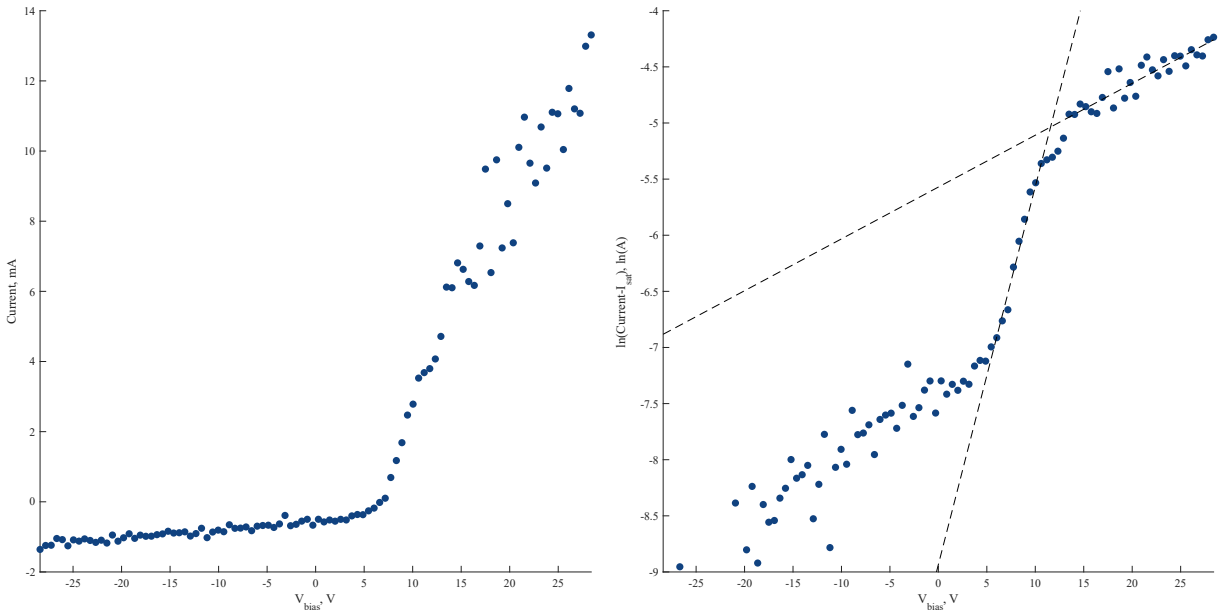

Figure 18. I-V curves generated from plasma created using adamantane as a fuel source.

The plasma parameters derived from the I-V curve are displayed in Table 1.

Table 1. Adamantane plasma parameters for the glass thruster.

Plasma Parameter	Measured Value
n_e, m^{-3}	$1.4 \cdot 10^{17} \pm 4 \cdot 10^{16}$
T_e, eV	3.0 ± 0.9
Φ_p, V	12 ± 0.2
Φ_f, V	6.9 ± 1.4

The results presented above confirm the effective ionization of the adamantane gas.

V. Data Analysis

Analyzing the thrust stand and Langmuir probe results, it was determined that the base thruster geometry was the most viable design due to its consistent, reliable behavior. However, further refinements in testing procedure and the lab's diagnostic suite may provide more comprehensive insight into all the thruster geometries.

The thrust stand data obtained for the base geometry provides an estimate of the thruster's efficiency. Thrust, F_t, for an electric propulsion thruster can be calculated using Equation 1,

$$F_t = \dot{m} v_e \tag{1}$$

where $\dot{m}$ is mass flow through the thruster and v_e is the exit velocity of the propellant. Furthermore, the mass flow can be represented by Equation 2,

$$\dot{m} = (I_i m_i)/q_i \tag{2}$$

where I_i is the ion beam current, m_i is the mass, and q_i is the charge of each ion. For adamantane, m_i is 136.2340 g/mol. Additionally, all ions were assumed to be singly charged as an approximation[14]. Exit velocity can be expressed as Equation 3,

$$v_e = \sqrt{(2q_i V_0)/m_i} \tag{3}$$

where V_0 is the potential between the electrodes in the thruster. Rearranging Equations 1, 2, and 3 results in an expression for the ion beam current as a function of the measured thrust, ion properties, and electric potential, shown in Equation 4.

$$I_i = F_t \sqrt{\frac{q_i}{2m_i V_0}} \tag{4}$$

The base resin thruster operated at a potential of 900 ± 80 V and thrust of 20 ± 6 μN, resulting in an estimated maximum ion current of 0.4 ± 0.1 mA. From the power supply, the applied current I_d was 2 mA. As a result, the current utilization efficiency, given by

$$\eta_b = \frac{I_i}{I_d} \tag{5}$$

was around 20%. This result indicates that the majority of the ions generated in the ionization chamber did not contribute to thrust. These ions were likely being accelerated directly into the cathode, creating the observed carbon deposits, rather than being accelerated out of the thruster. Only a small portion of ions successfully passed through the orifice, significantly reducing the thruster's efficiency. Other thruster geometries were designed to attempt to mitigate this inefficiency, either by enlarging the orifice to increase ion flux out of the thruster or by shrinking the cathode in the curved design to electrostatically accelerate the ions towards the orifice. However, these geometries must be further refined to achieve reliable ignition and stable operation before their performances can be compared with the base thruster.

Along with current utilization efficiency, propellant mass utilization efficiency can be examined. Linear drift observed in the thrust data indicates that propellant is lost before the thruster is ignited. The propellant that sublimates prior to ignition is lost without contributing to thrust, drastically reducing efficiency. Additionally, the increased drift observed during firing, indicating higher mass flow, suggests that a potential warm gas thrust might be present alongside the desired electrostatically induced thrust. This warm gas of neutral adamantane molecules would exit through the orifice at low velocities compared to the electrostatically accelerated ions, reducing equivalent exit velocity and thruster I_{sp}. In a companion paper, ASPEN simulated thruster operation, investigating the plasma environment in the ionization chamber and estimating thrust values. The simulations determined that an electrostatically induced thrust of 9 μN would be possible with the base thruster geometry. Based off that estimate, the direct measurements made with the thrust stand of 20 μN indicate that an 11 μN thrust was being produced by adamantane gas created during firing in addition to the adamantane ions. Due to the propellant's direct exposure to the plasma while in the propellant tank, interaction between the adamantane powder and the plasma during firing led to an increased sublimation rate and an unwanted warm gas thrust. Steps will need to be taken to control the mass flow to the ionization chamber to assist in reducing propellant waste and increasing I_{sp} by ensuring the thruster is operating entirely in an electrostatic condition.

While there is room to improve efficiency in the thruster, the Langmuir probe data obtained from the glass thruster offers a positive performance comparison to existing thruster technologies. Nauschütt et al. found that a radio frequency ion thruster had an electron density on the order of 10^{17} m^{-3} and an electron temperature on the order of 2-3 eV.[20] The electron density and temperature values calculated for ASPEN's thruster from the Langmuir probe data are similar to values obtained by commercially available thrusters, indicating that adamantane propellant is able to produce plasma similar to other fuels used in electric propulsion. Although ionization fraction is not directly measured, adamantane's electron density implies the fuel is able to ionize at a rate high enough to match other, more commonly used fuels.

Furthermore, the Langmuir probe data provides insight into the importance of material selection for the ASPEN thruster going forward. A glass or high-quality ceramic material must be used for future thruster designs to reduce contamination. Reducing unwanted carbon buildup within the thruster and plume is crucial for developing a reliable electric propulsion device.

VI. Future Work

Future development will focus on both the thruster and the ASPEN lab's diagnostic capabilities. The thruster will be redesigned to improve operational efficiency and work towards a form factor suitable for CubeSat integration. A

propellant feed system with an incorporated microvalve will be developed to control mass flow to the thruster, increasing propellant utilization efficiency by regulating sublimation and preventing propellant loss prior to ignition. Additionally, further investigation into the alternate geometries will be conducted to understand the conditions required for their stable operation. A comprehensive analysis of their performance will aid in understanding and increasing current utilization efficiency. Together, these improvements will enable a more rigorous evaluation of the ASPEN thruster's performance and advance the lab's goal of developing a low-cost CubeSat deorbiting system.

Subsequent designs will also utilize glass and ceramic materials, which offer significant advantages over the current resin thruster, including thermal resilience, low porosity, and minimal reactivity between the propellant and discharge environment. These materials offer the potential to reduce the formation of glass-like carbon and carbon-based contamination. Currently, a new thruster design is being manufactured with boron-nitride ceramic, an easily machined material commonly used for plasma contact areas in Hall thrusters. This material was originally avoided due to high material cost.

ASPEN also plans to expand its diagnostic suite to accommodate small thrusters that use molecular propellant, specifically by reducing probe invasiveness and developing equipment that is less sensitive to carbon deposits. Currently, a Faraday cup is being constructed that will provide a non-invasive method to characterize the thruster's ion beam current. The beam current data will provide information for validating numerical simulations, as well as informing electron density and temperature values. A double Langmuir probe is also in development. Furthermore, improvements to diagnostic procedures will provide measurements at higher temporal resolutions to better understand the plasma environment around the thruster. Additionally, thruster degradation from ion flux and other variations in thruster performance will be better documented with data provided by the new diagnostic equipment. Assisted by new diagnostic capabilities, ASPEN intends to continue to iterate to move towards a thruster suited for eventual CubeSat integration.

VII. Conclusion

This work demonstrates ASPEN's successful development of a torsional thrust stand and Langmuir probe, establishing a strong foundation for the lab's continued electric propulsion research. With these diagnostic tools, ASPEN performed a comparative study on various thruster geometries, evaluating their performance with adamantane as an unconventional solid propellant. In comparing the thruster geometries' performances, the lab determined that the base geometry was the most reliable, producing thrust of 20 ± 6 μN at an input power of 1.9 ± 0.3 W, with a current utilization efficiency of 20%. These results show an initial step towards active deorbit capabilities, though further development is required to increase efficiency by adding mass flow control and improving ion utilization. Furthermore, Langmuir probe measurements of electron density and temperature confirm that adamantane is readily ionized while also indicating that material choice is critical for future thruster designs to reduce unwanted contamination, such as carbon deposits and glass-like carbon formation. Overall, these results validate the possibility of adamantane as a compact solid propellant for CubeSat deorbit applications and they lay the groundwork for optimization to achieve performance for practical applications.

Acknowledgments

The authors would like to thank the members of the ASPEN Lab at the University of Southern California. The combined efforts of the lab members have been essential in the development of the thruster. The authors would also like to thank Professor Matthew Gilpin of the University of Southern California and Professor Lubos Brieda of California Polytechnic State University for their guidance, as this project would not have been possible without their insights. The authors thank the University of Southern California's Viterbi School of Engineering for its generous support, as well as Lockheed Martin, Boeing, and the Gammell Endowment for their sponsorship of the lab. We hope to continue our research and help the next generation of engineers gain critical skills with their continued support.

References

[1]Ostrom, C. and J. Opiela, "Orbital Debris Mitigation and Cubesats," NASA, 2021, https://ntrs.nasa.gov/api/citations/20210011558/downloads/Ostrom_OD%20Mitigation%20and%20CubeSats_final.pdf. Accessed 6 September 2025.

[2]Nagavarapu, S.C., Chandran, A., and Hastings, D.E. "Orbital Decay Analysis for Debris Deorbiting Cubesats in LEO: A Case Study for the Velox-II Deorbit Mission," *8th European Conference on Space Debris*, Vol. 8, No. 1, Accessed 3 September 2025.

[3]Mehta, S., Lugaz, N., and Thein, M., "An Evaluation of CubeSat Orbital Decay Utilizing ADCS" *SmallSat*, Vol. 1, Utah State University, Utah, 2024

[4]Sherpaili, P., R. Sah, S. Hegde, B. Chaudhary, "Design of Chemical Propellant Thruster to Deorbit Nano Satellite: StudSat-II," XVII Vibration Engineering & Technology of Machinery Conference, December 15-17, 2022, https://arxiv.org/pdf/2212.11992. Accessed 4 September 2025.

[5]Joergensen, F. and J. Snyder, "Search for a Trans-Disulfide: Structural Analysis of Di-Tert-Adamantyl Disulfide by Photoelectron Spectroscopy, Derivation of .Sigma.I(t-Ad), and Molecular Mechanics Calculations for Related Bulky Disulfides, " The Journal of Organic Chemistry, 1980, https://pubs.acs.org/doi/10.1021/jo01294a020. Accessed 19 August 2025.

[6]Mokbel, I., Ruzicka, K., Majer, V., Ruzicka, V., Ribeiro, M., Jose, J., & Zábranský, M., "Vapor Pressures and Thermal Data for Three High-Boiling Compounds of Petroleum Interest: 1-Phenyldodecane, (5α)-Cholestane, Adamantane," Fluid Phase Equilibria, 169(2), 191–207 (2000), DOI: 10.1016/S0378-3812(99)00342-8. Accessed 3 September 2025

[7]Dietz, P et al, "Molecular Propellants for Ion Thrusters," *Plasma Sources Sci. Technol*. 28 084001, 2019, https://iopscience.iop.org/article/10.1088/1361-6595/ab2c6c. Accessed 25 August 2025.

[8]Alnaqbi, S., Darfilal, D., Swei, S.S.M., "Propulsion Technologies for CubeSats: Review," *Aerospace*, 11(7), 502, 2024, DOI: 10.3390/aerospace11070502. Accessed 15 August 2025.

[9]Borrofors, A. N., Harding, D. J., Weissenrieder J., Ciaralli S., Hallock, A., Brinck, T., "Aromatic Hydrocarbons as Molecular Propellants for Electric Propulsion Thrusters," *Journal of Electric Propulsion*, Vol. 2, No. 24, 16 November 2023, DOI: 10.1007/s44205-023-00059-6. Accessed 20 August 2025.

[10]Tirila, V., Demaire A., Ryan C. N., "Review of Alternative Propellants in Hall Thrusters," *Acta Astronautica*, Vol. 212, November 2023, pp. 284-306, DOI: 10.1016/j.actaastro.2023.07.047. Accessed 21 August 2025

[11]Polk, J. E., Pancotti, A., Haag, T., King, S., Walker, M., Blakely, J., and Ziemer, J., "Recommended Practices in Thrust Measurements," International Electric Propulsion Conference, IEPC-2013-440, Washington, DC, Oct. 2013, https://hpepl.ae.gatech.edu/papers/2013_IEPC_Polk.pdf. Accessed 3 September 2025

[12]Gilpin, M. R., McGehee, W. A., Arnold, N. I., Natisin, M. R., and Holley, Z. A., "Dual-axis thrust stand for the direct characterization of electrospray performance," Review of Scientific Instruments, 93(6), 065102 (June 2022), DOI: 10.1063/5.0087716. Accessed 22 August 2025

[13]Li, P., Hershkowitz, N., Severn, G. "Building Langmuir Probes and Emissive Probes for Plasma Potential Measurements in Low Pressure, Low Temperature Plasmas." J. Vis. Exp. (171), e61804, https://doi.org/10.3791/61804 (2021). Accessed 1 September 2025

[14]Bouwman J., et al, "Spectroscopic Characterization of the Product Ions Formed by Electron Ionization of Adamantane," *National Library of Medicine*, 2018, https://pmc.ncbi.nlm.nih.gov/articles/PMC6392131/. Accessed 10 September 2025.

[15] Dietz, P., et al, "Status report of diamondoids as alternative propellants for ion-thrusters," International Electric Propulsion Conference, IEPC-2017-198, Atlanta, GA, Oct. 2017, https://electricrocket.org/IEPC/IEPC_2017_198.pdf. Accessed 4 September 2025

[16] Bretti, Michael A. "Progress and Developments of Ultra-Compact 10 Watt Class Adamantane Fueled Hall Thrusters for Picosatellites," International Electric Propulsion Conference, IEPC-2022-349, Cambridge, MA, Jun. 2022, https://appliedionsystems.com/wp-content/uploads/2022/06/IEPC-2022-349.pdf. Accessed 4 September 2025

[17]M. Umeno, M. Noda, H. Uchida, H. Takeuchi, "Deposition of DLC film from adamantane by using pulsed discharge plasma CVD," *Diamond and Related Materials,* Vol 17, No. 4-5, April 2008, pp. 684-687 https://www.sciencedirect.com/science/article/pii/S0925963508001428

[18]Coyne, D. "LIGO Vacuum Compatible Materials List," Ligo, 2013, https://dcc.ligo.org/public/0003/E960050/012/E960050-v12%20Vacuum%20Compatible%20Materials%20List.pdf. Accessed 27 August 2025

[19]Coen, C., Zaretsky, A., Gilpin, M, "Characterization of an Adamantane Thruster by a Langmuir Probe" *AIAA Region VI Student Conference*, Vol. 1, AIAA, Santa Clara, 2024. https://doi.org/10.2514/6.2024-80550. Accessed 1 September 2025

[20]Nauschütt, B.T., Chen, L., Holste, K. et al. Non-invasive assessment of plasma parameters inside an ion thruster combining optical emission spectroscopy and principal component analysis. EPJ Techn Instrum 8, 13 (2021). https://doi.org/10.1140/epjti/s40485-021-00070-x. Accessed 2 September 2025